ChemComm

COMMUNICATION

View Article Online
View Journal | View Issue

Cite this: *Chem. Commun.*, 2016, 52, 10755

Received 13th May 2016,
Accepted 1st August 2016

DOI: 10.1039/c6cc04032b

www.rsc.org/chemcomm

Plasma enhanced vortex fluidic device manipulation of graphene oxide†

Darryl B. Jones,* Xianjue Chen,‡ Alexander Sibley, Jamie S. Quinton, Cameron J. Shearer, Christopher T. Gibson and Colin L. Raston*

A vortex fluid device (VFD) with non-thermal plasma liquid processing within dynamic thin films has been developed. This plasma–liquid microfluidic platform facilitates chemical processing which is demonstrated through the manipulation of the morphology and chemical character of colloidal graphene oxide in water.

Fundamental challenges within the plasma processing community involve reducing emissions, improving energy efficiency and controlling processes on the micro- and nano-scales.[1] Plasma–liquid chemical processing[2] is emerging as a strong candidate to address these challenges. Here electrical breakdown in the presence of liquids can provide a source of radicals, photons, excited species, electrons and ions to initiate, participate in or catalyse chemical processes.[3] They have therefore found uses in the synthesis of carbon materials,[4–6] production of surfactant free nanoparticles,[7] and plasma–electrode electrochemistry.[8] However, most plasma–liquid applications have occurred with or within bulk solutions. For many plasma applications, the chemical processes occur at the interface between the plasma and liquid, where active species initiate a cascade of non-equilibrium processes as they interact with the liquid. The chemical mechanisms facilitated by the plasma–liquid interactions, such as nanoparticle growth, are then controlled or limited by diffusion. This has made the mixing of the bulk solution critical in controlling plasma–liquid chemical processes, such as producing size-uniform nanoparticles.[9] In attempts to improve plasma–liquid processing efficiency, rotating drum[10] and falling-film reactors[11] that create thin liquid films have been reported. Here the creation of thin films improves the plasma-treated surface to bulk ratio. These reactors have revealed the advantages of plasma-interactions with thin films by increasing the rate of degradation of persistent chemicals. However, in both of these reactors reducing the liquid film thickness has been undesirable as it reduces the liquid volume treatment rate. Moreover, the high operating cost and energy consumptions of these reactors has also limited the scope of their applications.[12]

In recent years, microfluidic and dynamic thin-film processing platforms have enabled novel applications in chemistry and biochemistry,[13] through their ability to control chemical reactivity and selectivity, and the manipulation of self-organised systems.[14] These technologies rely on controlling and manipulating fluids on micrometre scales. The vortex fluid device (VFD)[15] has emerged as a low-cost chemical processing platform for novel and improved chemical processing. Its applications have included refolding proteins,[16] decorating nanoparticles,[17] controlling chemical reactivity and selectivity,[18] slicing carbon nanotubes,[19] and improving the loading efficiency of vesicles for drug delivery.[20] Here small volumes of liquid are spun within a rapidly rotating tube with one end open that is tilted at an angle (θ) with respect to a horizontal axis. Dynamically-mixed thin liquid films are then generated in a controlled way through the rotational speed, tilt angle and fluid volume available, while mechanical vibrations can introduce Faraday waves into the fluid.[21] The properties of these thin liquid films are highly desirable for plasma liquid processing, as they address the inherent limitations and problems of plasma–liquid processing with bulk liquids. Further, as dynamic thin-film technologies assist in mass transport between the gas- and liquid-phases, they offer advantages in transporting active species formed in the plasma into the liquid. This may offer enhancements to the plasma–liquid processing capabilities.

In this paper we demonstrate plasma–liquid processing within dynamic thin liquid films in a vortex fluidic device. This technology is of broad interest to the wider chemical community as it offers opportunities to realise innovation through its distinct advantages and its potential to be adapted to a diverse range of plasma–liquid processing regimes. The prototype plasma thin liquid film technology is illustrated in Fig. 1. Here a 20 mm OD glass tube is rotated at speeds of up to 10 000 rpm.

Centre for Nanoscale Science and Technology, School of Chemical and Physical Sciences, Flinders University, GPO Box 2100, Adelaide, SA 5001, Australia.
E-mail: darryl.jones@flinders.edu.au, colin.raston@flinders.edu.au

† Electronic supplementary information (ESI) available. See DOI: 10.1039/c6cc04032b

‡ Present address: Center for Multidimensional Carbon Materials, Institute of Basic Sciences Center, Ulsan National Institute of Science and Technology, Republic of Korea.

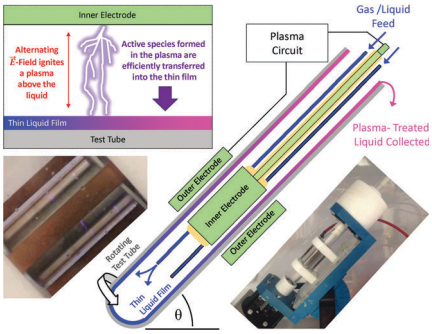

Fig. 1 A vortex fluidic device has been modified to enable plasma liquid processing with thin-liquid films. (insets) A schematic representation of the plasma generation above the liquid film, a photo of the device and the micro discharges observed during the plasma-processing.

A finite volume of liquid within the tube or a flow of liquid into the tube forms a vortex at the base of the tube to create a thin liquid film along the tube walls. A cylindrical stainless steel electrode (length 38 mm; 14 mm OD) is located within the tube, whilst a variable configuration brass electrode is located outside the tube. A plasma circuit generated high voltage (HV) negative pulses that were alternatingly applied to either the inner or outer electrode. This generates a pulsed alternating current (AC) electric field ($\vec{E}$-field) that ionizes the atmosphere above the film to produce a non-thermal plasma. This process is illustrated in Fig. 1, with an inset photo also showing the streamers (micro-discharges) ignited between the electrode and liquid film. The high mass transfer enhances active species formed in the plasma initiating or catalysing chemical processes within the thin liquid film, a feature unique to our technology. The large surface to bulk ratio, characteristic of thin liquid films, and its dynamic mixing within the device ensures that all of the liquid in the plasma region is exposed to the plasma. Furthermore, the variable rotational speed gives unprecedented control of the film thickness that is in contact with the plasma. In this way, the technology overcomes the limitation of plasma processing bulk solutions when the processes are driven through the plasma–liquid interface. The continuous mode of operation also facilitates uniform plasma exposure through the adjustment of liquid residence time within the active plasma region (liquid flow rate), whilst also being scalable for process intensification or suitable for assembly line syntheses.[22] The plasma properties can also be adapted through the chemicals in the solution and gas atmosphere, the available energy, and the pulse duration and repetition frequency. These parameters can manipulate the number and intensity of the micro-streamers, and the resultant activity of the plasma that drives chemical processes. This innovative technology therefore opens up a new research space for plasma chemical processing within thin-liquid films.

It is important to note that there has been recent interest in creating plasma-on-chip devices. These devices have enabled optical emission spectroscopy for trace metal detection,[23] and recently for treating individual cells in culture media.[24] These devices are still limited in scope through both the clogging inherent to channel based microfluidic platforms and problems relating to channel distortion and electrode damage from the plasma.[25] Our technology also overcomes these limitations.

To illustrate the utility of plasma processing in thin liquid films, as a novel and effective platform for chemical and material processing, we have investigated plasma–liquid processing of colloidal graphene oxide (G–O) in water. Since the discovery of the exceptional properties of graphene in 2004,[26] the modified forms of graphene have attracted intense research interest. Among them, G–O is undoubtedly one of the most important candidates, as it can be readily produced from inexpensive graphite in a relatively high yield, and it can be stably dispersed in a variety of solvents including water due to its amphiphilicity, thereby dramatically improving the processability of the atomically thin platelets for a wide range of applications.[27] Exploring the chemical properties of G–O requires controlling its morphology away from the purely two-dimensional form.[28] Indeed, physical deformation of the platelets, such as scrolls and crumples, might affect its chemical activity, especially along ripples or edges with high curvatures that would activate particular regions of atoms.[29] Manipulation of G–O is important for controlling its anti-fouling properties[30] and its role as a precursor in the production of graphene-based materials.[31] G–O is therefore a topical test case, furthered by efforts to process carbon materials using liquid plasmas.[4–6] We stress the innovative aspect of our approach in that G–O cannot usually be processed in channel-based microfluidic devices as it clogs the reactor. In addition, our technology also avoids the use of other toxic and hazardous chemicals for processing the G–O, highlighting the green chemistry nature of the technology.

In a typical experiment,§ 3 mL of 0.2 mg mL^{-1} G–O aqueous solution was plasma processed in the VFD using the confined mode of operation of the device with a rotational speed of 5000 rpm and $\theta = 45^{\circ}$. The plasma was generated through AC HV pulses ($\sim$17 kV, $f_{AC} \sim$ 830–910 Hz) that were repeated at a frequency of $\sim$230 Hz. The plasma treatment were performed in air with a peak power supplied at 42.5 W for 1 hour, or in nitrogen (N_2) with a peak power supplied at 75 W for 10 min. Here two distinct experimental condition were evaluated to demonstrate the versatility of the platform. The plasma thin film processing of colloidal G–O resulted in the formation of visible aggregates. It has been established that the colloidal stability of G–O is very sensitive to pH,[32,33] with a pH of 1 leading to large-scale visible aggregation and a pH of 14 yields a homogenous dark brown solution. The interaction of air and N_2 atmospheric pressure plasmas with liquid water is also known to influence the pH of the solution.[34] The plasma treatment of the thin-liquid film dropped the pH of the solution from 6 to 2 (air) or 3–4 (N_2). The visible aggregation of G–O from the plasma treatment is therefore consistent with this result.

In order to understand how the plasma–liquid treatment modified the G–O, the G–O properties were characterised using Transmission Electron Microscopy (TEM), Scanning Electron Microscopy (SEM), Atomic Force Microscopy (AFM), Scanning Auger Electron Microscopy, X-ray Photoelectron Spectroscopy (XPS) and Raman spectroscopy. An original as synthesised G–O has also been studied as a control. TEM images of the original G–O,

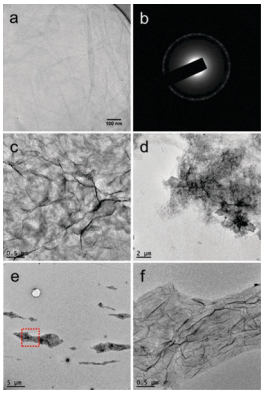

Fig. 2 TEM images of (a) original G–O sheets; (b) the corresponding selected area electron diffraction pattern acquired from the area in (a); (c and d) air-plasma treated G–O in H_2O; (e and f) plasma in N_2-atmosphere treated G–O in H_2O.

air-plasma and N_2-plasma treated G–O samples are shown in Fig. 2. Layers of stacked G–O can be seen in Fig. 2a, with the corresponding selected area electron diffraction pattern, Fig. 2b, indicating typical characteristics for stacked monolayer G–O sheets. Fig. 2c and d, revealed that the plasma-treatment of the G–O in air induced a morphology change through a crumpling of the G–O sheets. The morphology of the samples was further characterised using a combination of SEM and AFM imaging (Fig. 3). This crumpling seen in the air plasma treated G–O is reflected by pronounced ripples that alter the topography compared to the flat control. These ripples increased the average roughness of the sample (R_a = 48.5 ± 7.4 nm) by a factor of 5 from that of the control (R_a = 9.9 ± 0.8 nm). Chemical information about the samples was investigated using Auger spectromicroscopy with elemental mapping of the areas examined using SEM (Fig. 3) and XPS and Raman spectroscopy (Fig. 4). The scanning Auger images highlight the uniformity of the C/O ratio in the control, while the C/O maps for the air plasma treated G–O indicated some surface fluctuations that mimic the wrinkling observed in the SEM image. The elemental composition of the G–O films was further investigated using Auger spectroscopy, with the basal plane C/O ratios of 4.6 ± 1.8, 12.8 ± 4.8, and 4.5 ± 1.3 being observed for the control, air-plasma and N_2-plasma respectively. This observation is complementary to the XPS C1s analysis where the total percentage of carbon existing in oxygen environments are 39.3% (original G–O), 27.8% (air plasma) and 40.5% (N_2 plasma). This suggests that the low power, 1 hour air-plasma treatment of G–O in H_2O can partially reduce the G–O, converting CO environments into CC/CH environments. The Raman spectra suggest that this air-plasma treatment doesn't substantially alter the I_G/I_D band intensity ratio from the control sample. While the sample is partially reduced, the wrinkled nature doesn't facilitate repair of sp^3 to sp^2 bonding, and the intensity of the D band is preserved.[35] Unfortunately the non-uniformity of the deposited films doesn't facilitate further surface characterisations, such as contact angle.

The G–O plasma-treated in a N_2 atmosphere at higher plasma power, but shorter treatment time, displays a different

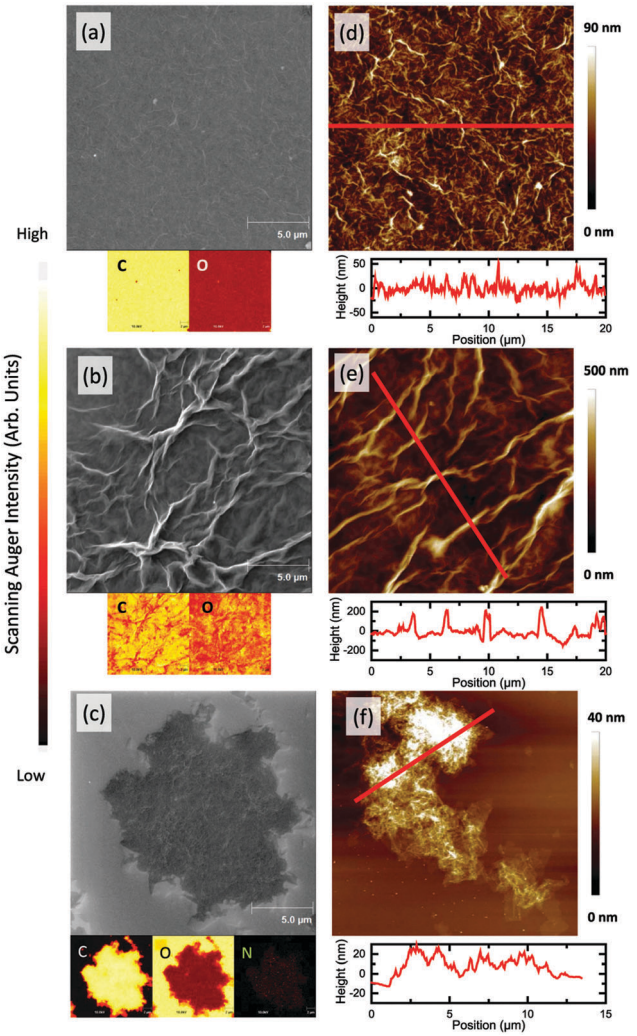

Fig. 3 Scanning electron images and Auger elemental maps [C, O and N (if present)] of (a) control, (b) air-plasma treated, and (c) N_2-plasma treated G–O. AFM images (20 × 20 μm) and height profiles of (d) control, (e) air-plasma treated, and (f) N_2-plasma treated G–O. The Auger maps are taken in the same location as the SEM images. The lines within the AFM images indicate the location of the height profile.

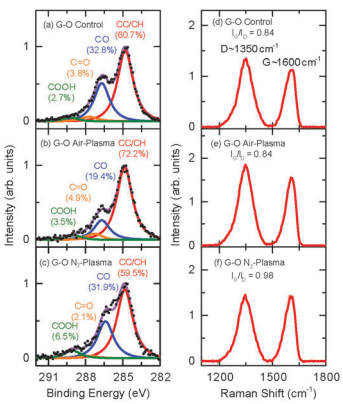

Fig. 4 High resolution C1s XPS for (a) control, (b) air-plasma treated, (c) N_2-plasma treated G–O. Raman spectra of (d) control, (e) air-plasma treated, and (f) N_2-plasma treated G–O.

morphology change, where it appears that the sheets wrap around themselves to form individual clusters, Fig. 2e and f. The localised influence of the filamentary discharges within the higher power N_2 plasma may induce phenomenologically similar behaviour to microwave spark scrolling of graphene.[36] Here the C/O ratio is not substantially changed from the control. However, Raman spectroscopy indicates that the G–O I_G/I_D ratio increases with a high intensity N_2-plasma treatment. This plasma treatment may facilitate platelets breaking on sp^3 defects to create the individual folded clusters, increasing the relative number of $G(sp^2)/D(sp^3)$ domains. The folding/breaking may influence the edge structure to partially suppress the D band, as occurs in graphene.[37] The Auger spectral data also suggest that the N content in the G–O may increase through the N_2 plasma treatment.

Lastly, upon inspection of the surface morphologies for the air and N_2 atmospheric pressure plasmas treated G–O, we note that it is different to that observed when G–O solution was pH adjusted by adding HCl, where in that case the G–O sheets folded and assemble into larger packed structures.[33] The localised plasma effects within the thin liquid film may therefore produce morphology changes different from those achieved through pH adjustment of bulk solution. The versatility for materials modification with our technology was further revealed through unique manipulations of G–O morphologies and chemical character with different plasmas chemistries. This highlights the novel processing capabilities of plasma thin-film technologies.

We have developed a processing platform that facilitates novel plasma chemical processing using thin-liquid films, and demonstrate that coupling plasma–liquid interactions into thin film devices can enhance chemical processing and materials manipulation. Further investigations will consider how adjusting the plasma and thin film properties may assist in controlling material synthesis, and extending the work into continuous flow studies. They will also include characterisation of the plasma–liquid interactions with thin-films.

We acknowledge financial support provided by the Government of South Australia and the Australian Research Council [DECRA (DBJ), Discovery grants (CLR), and LIEF (JSQ)]. This work was facilitated by the Technical Services Unit and Australian Microscopy and Microanalysis Research Facility (AMMRF) at Flinders University.

Notes and references

§ Methods summary: full details of methods and analysis are contained in the ESI.†

1 K. Bazaka, M. V. Jacob and K. Ostrikov, *Chem. Rev.*, 2016, **116**, 163–214.
2 S. Samukawa, M. Hori, S. Rauf, K. Tachibana, P. Bruggeman, G. Kroesen, J. C. Whitehead, A. B. Murphy, A. F. Gutsol, S. Starikovskaia, U. Kortshagen, J.-P. Boeuf, T. J. Sommerer, M. J. Kushner, U. Czarnetzki and N. Mason, *J. Phys. D: Appl. Phys.*, 2012, **45**, 253001.
3 E. C. Neyts, K. Ostrikov, M. K. Sunkara and A. Bogaerts, *Chem. Rev.*, 2015, **115**, 13408–13446.
4 J. Kang, O. L. Li and N. Saito, *Carbon*, 2013, **60**, 292–298.
5 J. Senthilnathan, Y.-F. Liu, K. S. Rao and M. Yoshimura, *Sci. Rep.*, 2014, **4**, 4395.
6 H. Lee, M. A. Bratescu, T. Ueno and N. Saito, *RSC Adv.*, 2014, **4**, 51758–51765.
7 D. Mariotti, J. Patel, V. Švrček and P. Maguire, *Plasma Processes Polym.*, 2012, **9**, 1074–1085.
8 C. Richmonds and R. M. Sankaran, *Appl. Phys. Lett.*, 2008, **93**, 131501.
9 X. Z. Huang, X. X. Zhong, Y. Lu, Y. S. Li, A. E. Rider, S. A. Furman and K. Ostrikov, *Nanotechnology*, 2013, **24**, 095604.
10 H. Krause, B. Schweiger, E. Prinz, J. Kim and U. Steinfeld, *J. Electrost.*, 2011, **69**, 333–338.
11 B. P. Dojčinović, G. M. Roglić, B. M. Obradović, M. M. Kuraica, M. M. Kostić, J. Nešić and D. D. Manojlović, *J. Hazard. Mater.*, 2011, **192**, 763–771.
12 B. Jiang, J. Zheng, S. Qiu, M. Wu, Q. Zhang, Z. Yan and Q. Xue, *Chem. Eng. J.*, 2014, **236**, 348–368.
13 G. M. Whitesides, *Nature*, 2006, **442**, 368–373.
14 X. Chen, N. M. Smith, K. S. Iyer and C. L. Raston, *Chem. Soc. Rev.*, 2014, **43**, 1387–1399.
15 L. Yasmin, X. Chen, K. A. Stubbs and C. L. Raston, *Sci. Rep.*, 2013, **3**, 2282.
16 T. Z. Yuan, C. F. G. Ormonde, S. T. Kudlacek, S. Kunche, J. N. Smith, W. A. Brown, K. M. Pugliese, T. J. Olsen, M. Iftikhar, C. L. Raston and G. A. Weiss, *ChemBioChem*, 2015, **16**, 393–396.
17 Y. A. Goh, X. Chen, F. M. Yasin, P. K. Eggers, R. A. Boulos, X. Wang, H. T. Chua and C. L. Raston, *Chem. Commun.*, 2013, **49**, 5171–5173.
18 J. Britton, J. M. Chalker and C. L. Raston, *Chem. – Eur. J.*, 2015, **21**, 10660–10665.
19 K. Vimalanathan, J. R. Gascooke, I. Suarez-Martinez, N. A. Marks, H. Kumari, C. J. Garvey, J. L. Atwood, W. D. Lawrance and C. L. Raston, *Sci. Rep.*, 2016, **6**, 22865.
20 J. Mo, P. K. Eggers, X. Chen, M. R. H. Ahamed, T. Becker, L. Yong Lim and C. L. Raston, *Sci. Rep.*, 2015, **5**, 10414.
21 J. Britton, S. B. Dalziel and C. L. Raston, *Green Chem.*, 2016, **18**, 2193–2200.
22 J. Wegner, S. Ceylan and A. Kirschning, *Adv. Synth. Catal.*, 2012, **354**, 17–57.
23 Y. Kohara, Y. Terui, M. Ichikawa, K. Yamamoto, T. Shirasaki, K. Kohda, T. Yamamoto and Y. Takamura, *J. Anal. At. Spectrom.*, 2015, **30**, 2125–2128.
24 S. Kumagai, C.-Y. Chang, J. Jeong, M. Kobayashi, T. Shimizu and M. Sasaki, *Jpn. J. Appl. Phys.*, 2016, **55**, 01AF01.
25 C.-Y. Chang, M. Sasaki, S. Kumagai and G.-J. Wang, *J. Phys. D: Appl. Phys.*, 2016, **49**, 155203.
26 A. K. Geim and K. S. Novoselov, *Nat. Mater.*, 2007, **6**, 183–191.
27 D. R. Dreyer, S. Park, C. W. Bielawski and R. S. Ruoff, *Chem. Soc. Rev.*, 2010, **39**, 228–240.
28 R. Ruoff, *Nature*, 2012, **483**, S42.
29 D. Srivastava, D. W. Brenner, J. D. Schall, K. D. Ausman, M. Yu and R. S. Ruoff, *J. Phys. Chem. B*, 1999, **103**, 4330–4337.
30 M. Hu, S. Zheng and B. Mi, *Environ. Sci. Technol.*, 2016, **50**, 685–693.
31 S. Pei and H.-M. Cheng, *Carbon*, 2012, **50**, 3210–3228.
32 C.-J. Shih, S. Lin, R. Sharma, M. S. Strano and D. Blankschtein, *Langmuir*, 2012, **28**, 235–241.
33 R. L. D. Whitby, A. Korobeinyk, V. M. Gun'ko, R. Busquets, A. B. Cundy, K. Laszlo, J. Skubiszewska-Zieba, R. Leboda, E. Tombacz, I. Y. Toth, K. Kovacs and S. V. Mikhalovsky, *Chem. Commun.*, 2011, **47**, 9645–9647.
34 P. Rumbach, M. Witzke, R. M. Sankaran and D. B. Go, *J. Am. Chem. Soc.*, 2013, **135**, 16264–16267.
35 Y. Hu, S. Song and A. Lopez-Valdivieso, *J. Colloid Interface Sci.*, 2015, **450**, 68–73.
36 J. Zheng, H. Liu, B. Wu, Y. Guo, T. Wu, G. Yu, Y. Liu and D. Zhu, *Adv. Mater.*, 2011, **23**, 2460–2463.
37 M. Begliarbekov, O. Sul, S. Kalliakos, E.-H. Yang and S. Strauf, *Appl. Phys. Lett.*, 2010, **97**, 031908.

